Implications of sepiolite dehydration for earthquake nucleation in the Galera Fault Zone: a thermodynamic approach

Catalina Sánchez-Roa[1], Olivier Vidal[2], Juan Jiménez-Millán[1], Fernando Nieto[3], Daniel R. Faulkner[4]

[1] Departamento de Geología and CEACTierra, Unidad Asociada IACT (CSIC-UGR), Universidad de Jaén, Campus Las Lagunillas s/n 23071, Jaén, Spain.

[2]Isterre, CNRS, Université Grenoble Alpes

1381 rue de la piscine, BP 53, 38041 Grenoble Cedex, France.

[3] Departamento de Mineralogía y Petrología and IACT (CSIC-UGR), Facultad de Ciencias, Universidad de Granada, Avda. Fuentenueva s/n 18002, Granada, Spain.

[4] Rock Deformation Laboratory, Department of Earth and Ocean Sciences, University of Liverpool, Liverpool, UK.

Running head: Thermodynamic modelling of sepiolite dehydration

*E-mail: catasroa@ujaen.es

ABSTRACT

A new thermodynamic model for the Mg-phyllosilicate sepiolite was developed and used to calculate its P-T stability conditions and water content for different bulk rock compositions. The standard-state thermodynamic properties, entropy (S°) and enthalpy (H°), were initially estimated by oxide summation taking into account the different entropic and enthalpic contributions of the three types of water in sepiolite: zeolitic water, bound water, and structural OH groups. The starting model was then refined with experimental data. The dehydration process follows a step function that allowed us to define "end-members" with decreasing hydration states in a theoretical solid solution.

The stability field of sepiolite is ultimately limited by the reaction sepiolite = talc + quartz + H_2O, which is located at about 325°C at 1 to 500 MPa. The large stability field of this clay mineral suggests that it could control the mechanical behaviour of crustal faults to

325°C. The refined model was then applied to the natural case of the Galera Fault Zone (SE Spain) using thermogravimetric analysis and X-ray fluorescence data of the bulk rock composition of the fault core gouge, which is mainly composed of sepiolite. The dehydration of sepiolite at T < 300°C is modest compared to that occurring during its breakdown, where 62% of water molecules leave the structure to form the association talc + quartz + H_2O; a reaction that also involves a reduction of around 31% of the original solid volume. These significant hydration and volume changes of sepiolite can have important implications on the strength and mechanical stability of the Galera Fault and other sepiolite-bearing gouges. We compare triaxial friction experiments on the natural sepiolite-rich gouge with a synthetic gouge to estimate strength changes on the gouge with depth. The synthetic gouge represents the breakdown association above 325°C, and was constructed following the mineral phases predicted by the thermodynamic model (93 wt% talc and 7 wt% quartz). The contrasting frictional strength and mechanical stability of sepiolite in comparison to talc could be one of the causes of fault instability and earthquake nucleation seen to be concentrated in the upper 13 km of the Galera Fault.

Keywords: sepiolite, thermodynamic modelling, friction experiments, fault gouge, earthquake nucleation, dehydration, Galera Fault.

1. INTRODUCTION

Phyllosilicates are abundantly found within active fault systems, where their crystallographic structure retains large amounts of water (Haines and van der Pluijm, 2012; Morton et al., 2012; Richard et al., 2014; Schleicher et al., 2012; Yalçin and Bozkaya, 2004). The presence of water, both within the crystals and on their main cleavage planes, often results in the low strength of clay-rich fault zones (Lockner et al., 2011; Schleicher et al., 2013). By facilitating slip and distributing water within active faults, clay minerals play an important role in the mechanics of earthquakes.

Clay mineral dehydration in active fault systems requires a complex reorganisation of water molecules. Controlled humidity chamber experiments have shown that water layers in smectite occur at seismogenic depths, and that humidity in this context also affects particle orientation (Schleicher et al., 2013). The hydration state and particle orientation of clay minerals in active fault systems suggest greater mobility of the particles, which has important effects on frictional strength of fault gouges (Moore and Lockner, 2007; Schleicher et al., 2013). Furthermore, numerical simulations of pore pressure within fault zones have linked the onset of dehydration reactions in fault systems to instabilities on the fault plane. This leads to a transient acceleration of the fault motion, which stops when the reaction is finished but that can strongly modify the nucleation of unstable slip (Brantut et al., 2011). The evolution of fault strength and its relation to the seismic cycle requires the observation of natural systems to evaluate the extent of competing mechanisms such as fracturing and healing. These mechanisms are strongly dependent on the geological context, including the mineralogy and fluid flow in the area, which consequently are controlling factors on important processes within fault zones such as creep, mass transfer and pressure solution (Gratier, 2011).

Fibrous clay minerals commonly occur within fracture and fault zones (Post and Crawford, 2007; Sánchez-Roa et al., 2016), occasionally constituting the major portion of fault gouges in active faults. Thus, the study of the role of fibrous phyllosilicates becomes crucial to understand their relationship to earthquake dynamics. Sepiolite is a fibrous clay mineral that can occur as a product of weathering of ophiolitic bodies (Gleeson et al., 2004; Ratié et al., 2015) and related to other Mg-rich minerals with important roles in fault stability such as saponite, minerals from the serpentine group, and talc (Manning, 1995; Yalçin and Bozkaya, 2004). Sepiolite is found associated with fault zones and fault planes (Haines and van der Pluijm, 2012; Sánchez-Roa et al., 2016). Therefore, the study and modelling of the hydration state, mineral reactions, as well as the chemical and mechanical stability of sepiolite are key steps towards understanding the mechanical behaviour of sepiolite-rich fault gouges.

Sepiolite is composed of continuous silica tetrahedral sheets with the apical oxygen periodically inverted and a discontinuous octahedral layer between them (García-Romero and Suárez, 2013). Due to these periodical inversions, sepiolite has a fibrous morphology and channels containing H_2O molecules. These channels can also accommodate some organic molecules and exchangeable cations (which are not bound to the structure) such as Na^+, K^+, and Ca^{2+} (Krekeler and Guggenheim, 2008). Sepiolite is a hydrated Mg-rich fibrous phyllosilicate with ideal formula: $Si_{12}Mg_8O_{30}(OH)_4(OH_2)_4 \bullet 8(H_2O)$. It contains three crystal-chemical states of water molecules: zeolitic water in the channels; bounded water completing the coordination of Mg^{+2} atoms in the edges of the octahedral layers; and hydroxyl groups (OH^-) in the octahedral layer (Brauner and Preisinger, 1956). Experimental data has shown that dehydration of sepiolite consists of various stages containing step functions (Nagata et al., 1974; Post et al., 2007). First, most of the zeolitic water is lost when heated to 117°C or at room temperature under a vacuum of 1.33×10^{-4} Pa. No change in the unit cell had been recognised until Rietveld refinements of temperature-resolved

synchrotron powder X-ray diffraction data showed a slight decrease in the *a* (decrease of ~1.2%) and *c* (decrease of ~0.2%) unit cell parameters during this stage (Post et al., 2007). This structure corresponds to the sepiolite-4H_2O end-member. The loss of the bounded water takes place in two subsequent stages that are accompanied by the folding of the sepiolite structure and formation of the experimentally achieved sepiolite-2H_2O and sepiolite-0H_2O (a high temperature structure that retains the hydroxyl groups) (Nagata et al., 1974; Post et al., 2007).

The presence of sepiolite in the fault gouge of active faults and its hydration properties lead us to seek appropriate tools to discover the way sepiolite behaves under changing chemical and physical conditions. Currently there is a shortage of data on the evolution of this fibrous clay mineral in nature, including sepiolite interactions and compatibility relations with other phases in a wide range of pressure and temperature conditions. To date, progress has been made to estimate the thermodynamic properties of fully hydrated and dehydrated sepiolite (Wolery and Jove-Colon, 2004; Ogorodova et al., 2014). However, these estimations have not yet entirely described the whole dehydration range of sepiolite or the mineral reactions involved in geological processes within the Earth's crust. The scarcity of data on sepiolite stability and mineral transformations can be approached from a thermodynamic perspective.

Thermodynamic models constrained by experimental data are used in this study to assess the extent of sepiolite contributions to fault mechanics and earthquake nucleation. The refined model is applied to the natural case of the Galera Fault, which has a sepiolite-rich fault gouge produced by hydrothermal alteration of Mg-rich fluids during periods of fluid-rock interactions that concentrated on fault planes and fractures of the deformation area. XRD data limitations in determining the accurate percentage of sepiolite in the rock are mitigated by performing a thermogravimetric analysis of the fault rock that can confirm sepiolite is the major constituent of the gouge and an optimum candidate to assess the

water release, volume changes and mineral reactions that can take place on Galera Fault's active fault planes during ongoing deformation. Previous experimental work on the mechanical properties of the Galera fault gouge showed the strength of the sepiolite-rich gouge to have friction coefficients around 0.47 under water-saturated conditions (Sánchez-Roa et al., 2016). To assess the changes on fault strength in the Galera Fault with changing pressure and temperature, we compare the experimentally-measured friction coefficient of the sepiolite-rich gouge with experimental strength measurements of the friction coefficient of a synthetic gouge mixture based on the mineral assemblage and proportions predicted by the newly proposed thermodynamic model.

This study presents the integration of a new thermodynamic model for sepiolite with frictional tests assessing fault strength, and the application of these methods to a natural example as a strategy to explore the relation between sepiolite dehydration and earthquake nucleation in the Galera Fault Zone.

2. THERMODYNAMIC MODEL

2.1 Considered range of hydration states

Synchrotron XRD data show that the volume vs temperature dehydration curve of sepiolite is a step function (Post et al., 2007), similar to that observed for smectite dehydration. In smectite, this step dehydration results from two different processes: i) continuous loss of interlayer water and constant decrease of volume for a fixed number of water layers, and ii) discontinuous loss of water layers and large volume changes associated with the collapse of the interlayer space at fixed temperatures (see Vidal and Dubacq, 2009 and references therein). Similarly, the step dehydration in sepiolite results from the progressive loss of interlayer water (zeolitic water), as well as the folding of the sepiolite structure that can be compared to the collapse of the interlayer space for smectites. Five end-members with different hydration states (including zeolitic and bound water molecules) and four solid solutions between these end-members must be defined to cover the entire range of possible sepiolite hydration from 12 to 0 H_2O p.f.u: Sepiolite-12H_2O, Sepiolite-6H_2O, Sepiolite-4H_2O, Sepiolite-2H_2O, and Sepiolite-0H_2O (Fig. 1). However, given the lack of thermodynamic stability of the experimentally achieved sepiolite-2H_2O and the sepiolite-0H_2O, as well as their absence in nature, we restricted our study and thermodynamic model to the "zeolitic water". Following the approach proposed for smectite by Vidal and Dubacq (2009), the step dehydration of sepiolite was modelled with two solid solutions between the zeolitic-water-free end-member Sepiolite-4H_2O and the end-members Sepiolite-12H_2O or Sepiolite-6H_2O. The Fe-Mg compositional variation in sepiolite was not included in this model due to the few occurrences of Fe-sepiolite and the lack of Fe-Mg exchange in the studied samples. The exchangeable cations within the channels were also excluded from the model assuming that their contributions are negligible compared to the major differences between the three types of water in the structure, thus they are not expected to affect the dehydration temperatures of sepiolite.

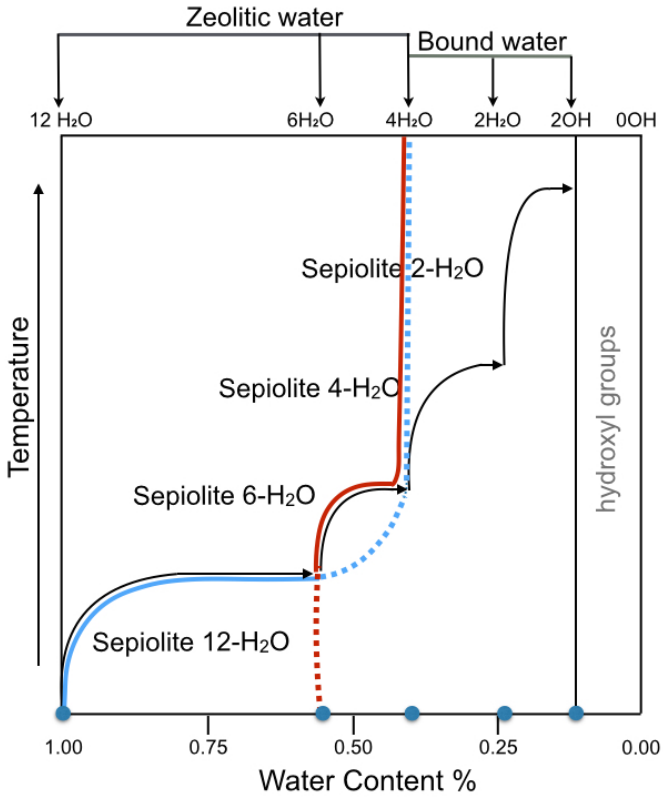

Figure 1. Dehydration model of sepiolite with temperature considering XRD data of the dehydration curve of sepiolite from Post et al. (2007) and the dehydration model proposed by Vidal and Dubacq (2009). The water content of the end-members is shown with circles in the horizontal axis both as water% and moles of water. The black lines indicate the experimentally proven transitions and the end-members initially considered. The blue and red lines indicate the solid solutions selected for the model, where the dashed parts of the lines indicate the metastable parts.

2.2 Thermodynamic approach

In view of the strong similarities with smectite, the thermodynamic model developed for sepiolite in the present study follows a similar method to that proposed for smectite by Vidal and Dubacq (2009). The hydration state of sepiolite is calculated by solving the conditions of the two following equilibria between two different hydrous end-members and the same end-member without zeolitic water (Sepiolite.4H_2O) at fixed P, T and aH_2O:

$$Sepiolite.12H_2O = Sepiolite.4H_2O + 8H_2O \quad (1)$$

$$Sepiolite.6H_2O = Sepiolite.4H_2O + 2H_2O \quad (2)$$

The conditions of equilibria 1) and 2) for $aH_2O = 1$ read:

$$RTln(aSepiolite.4H_2O/aSepiolite.12H_2O) = \Delta G(1)_f^{P,T} \quad (3)$$

$$RTln(aSepiolite.4H_2O/aSepiolite.6H_2O) = \Delta G(2)_f^{P,T} \quad (4)$$

Where a stands for activity and

$$\Delta G_f^{P,T} = G^{P,T}Sepiolite.4H_2O - G^{P,T}Sepiolite.12H_2O + 8G^{P,T}H_2O \quad \text{or}$$

$$= G^{P,T}Sepiolite.4H_2O - G^{P,T}Sepiolite.6H_2O + 2G^{P,T}H_2O$$

Where:

$$\Delta G_f^{P,T} = \Delta H_f^{1,298} - T\Delta S^{1,298} + \int_{298}^{T} \Delta Cp\partial T - T\int_{298}^{T} \Delta Cp/T\,\partial T + \int_{1}^{P} \Delta V\partial P \quad (5)$$

The activities of the sepiolite end-members were assumed to be equal to their molar fraction (ideal solid solution model). Under this assumption, the molar fractions of $Sepiolite.4H_2O$ in the solid solution between $Sepiolite.4H_2O$ ($X_{4,1}$) and $Sepiolite.12H_2O$ or between $Sepiolite.4H_2O$ ($X_{4,2}$) and $Sepiolite.6H_2O$ can be calculated as:

$$X_{4,1}/(1-X_{4,1}) = \exp(\Delta G(1)_f^{P,T}/RT) \quad (6)$$

$$X_{4,2}/(1-X_{4,2}) = \exp(\Delta G(2)_f^{P,T}/RT) \quad (7)$$

The relative stability of the two solid solutions and the water content of sepiolite were calculated at given P and T from equilibria (6) and (7). Thermodynamic calculations of the stepwise dehydration of sepiolite, and its stability and compatibility relations were calculated by Gibbs free energy minimisation using Theriak-Domino (de Capitani, 1994; de Capitani and Brown, 1987; de Capitani and Petrakakis, 2010)

(http://titan.minpet.unibas.ch/minpet/theriak/theruser.html) after implementation of the thermodynamic properties of sepiolite end-members discussed below, and with the thermodynamic properties of common rock-forming minerals included in the internally consistent database jun92.bs (version c), an update of the initial dataset of Berman et al. (1988). The thermodynamic properties of smectite end-members included in Vidal and Dubacq (2009) were also incorporated to the calculations of selected natural samples. The electronic database containing the thermodynamic properties derived in this study and used for calculations of sepiolite-rich samples can be found in the supplementary information (electronic file 1).

2.3 Estimation of thermodynamic properties

The molar volume of sepiolite was calculated for its different hydration states based on the cell dimensions reported in the Rietveld refinement process for the sepiolite structure detailed in Post et al. (2007). Other thermodynamic properties of sepiolite-12H_2O, -6H_2O and -4H_2O end-members were first approximated using oxide summation techniques:

-The heat capacity functions of all sepiolite end-members were calculated according to the equation of Berman and Brown (1985):

$$Cp = k_1 + k_2 \cdot T + \frac{k_3}{T^2} + \frac{k_4}{\sqrt{T}} + k_5 \cdot T^2 + \frac{k_6}{T} + k_7 \cdot \sqrt{T} + \frac{k_8}{T^3} + k_9 \cdot T^3 \; [J/mol]$$

The V(P, T) function of sepiolite was assumed to be the same as that of muscovite.

- The standard-state third-law entropies (S°) of sepiolite end-members were estimated using the additivity of oxide components procedure (Holland, 1989). The value of $(S\text{-}V)_{H2O}$ was fixed for zeolitic water = 39 J/mol/K, lower than the first approximation of the standard entropy of interlayer H_2O reported to be 55 J/mol/K (Ransom and Helgeson, 1994). However, 39 J/mol/K shows the best fit for the dehydration model in a binary system of water activity vs temperature (Fig. 2a). The OH groups from the octahedral sheet were assigned with a value of S° equals 7.44 J/mol/K according to Holland (1989), taking into account that sepiolite has a trioctahedral structure and the

three full octahedral sites repel the proton equally (Bailey, 1984). Finally, the value for bounded water was arbitrarily fixed to 28 J/mol/K, as an intermediate value that provides a significant distinction between the different entropy contributions of the three different types of water within the sepiolite structure.

- A first estimation of the 1 bar, 25°C enthalpy of formation of sepiolite end-members was made according to the oxide summation technique of Chermak and Rimstidt (1989), which has been proven to give good first approximations for clay minerals (Vidal and Dubacq, 2009).

Two sets of thermodynamic properties were derived in this study by varying the calculated values of enthalpy of formation and repeatedly calculating the model output of reaction curves. The aim was to: 1) achieve the best possible fit of the dehydration vs temperature evolution of Post et al. (2007) obtained by Rietveld refinements of temperature-resolved synchrotron powder X-ray diffraction data, and 2) create a realistic stability field for sepiolite while adjusting its stability conditions compared to talc in presence of quartz and water. This second objective relied on cold-seal pressure vessel experiments reported by Frank-Kamenetskiy et al. (1969) showing that sepiolite breaks down into talc, quartz and water at 325°C for pressures between 1 and 300 MPa.

Figure 2 presents the binary diagrams of reactions described by equations 1 and 2 for the two sets of thermodynamic properties derived in this study (Fig. 2a and 2b). The reactions occur between the three end-members of hydration (Sepiolite-12H_2O, Sepiolite-6H_2O and Sepiolite-4H_2O) using two solid solutions. The first solid solution from Sepiolite-12H_2O to Sepiolite-4H_2O end-members and the second from Sepiolite-6H_2O to Sepiolite-4H_2O end-members. The results of this calculation are compared with the experimental dehydration data reported in Post et al. (2007) for the progressive dehydration of sepiolite.

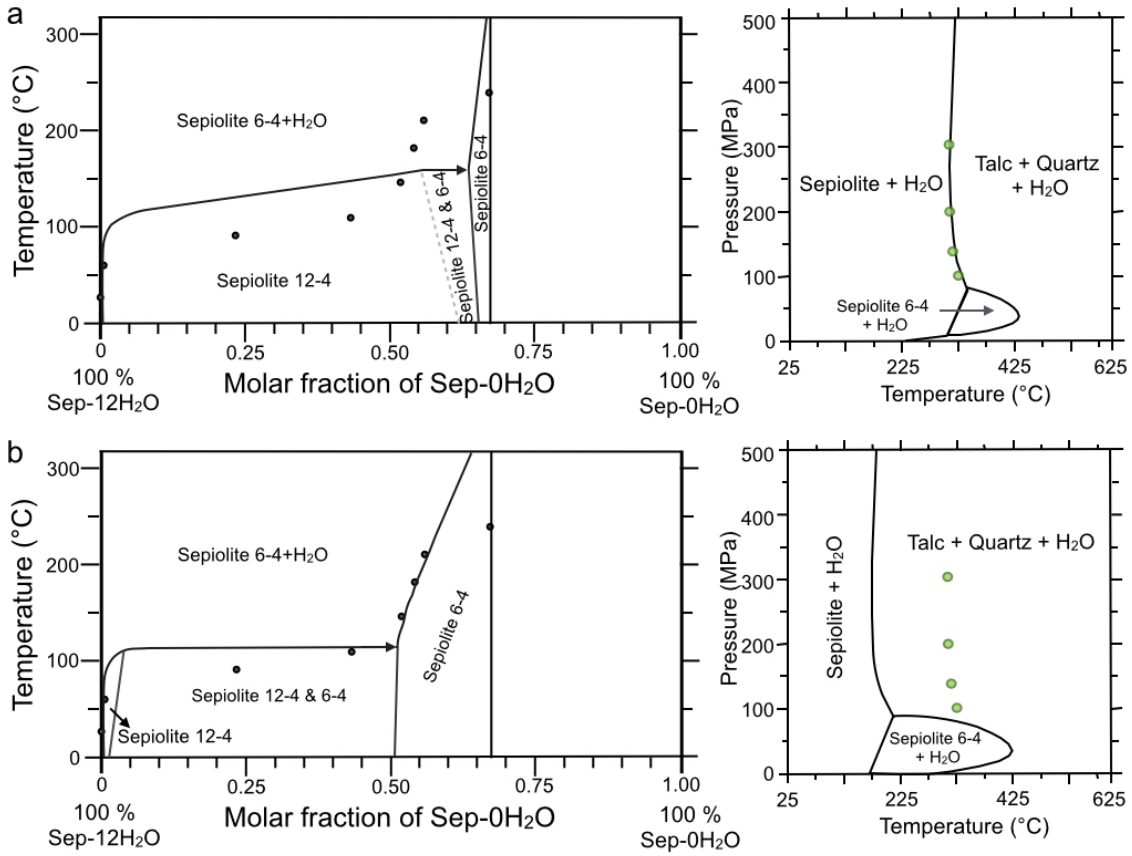

Figure 2. Binary phase diagrams of water content in the sepiolite structure versus temperature showing the progressive dehydration of sepiolite. Black dots represent the results of Rietveld refinement of the dehydration process (Post et al., 2007) and green dots correspond to the experimentally determined limit of reaction sepiolite = talc + quartz + H_2O by Frank-Kamenetskiy et al. (1969). The continuous black line is the output of this model. **a.** Using the standard-state thermodynamic properties derived in this study and adjusted to fit the phase transformation experimental data (Frank-Kamenetskiy et al., 1969), this set of thermodynamic properties are presented in Table 1. Right-hand side: simplified P-T phase diagram with the reaction curves for model a. **b.** Using adjusted standard-state thermodynamic properties to achieve a better agreement with the dehydration of sepiolite at low temperature. Right-hand side: simplified P-T phase diagram with the reaction curves for model b.

The two sets of thermodynamic properties aim to find the best fit for both sets of experiments, namely, Post et al. (2007) and Frank-Kamenetskiy et al. (1969). The reaction curves shown in figure 2a are not the closer model fit for the refinement data (Post et al., 2007), a better fit for these dehydration data is possible using a second set of adjusted thermodynamic properties of the sepiolite end-members (Fig. 2b). Nevertheless, this study favours the first set of properties (Fig. 2a), which provides a better fit for the experimentally supported phase reactions presented in Frank-Kamenetskiy et al. (1969) that were obtained including pressure as a factor. Only this set of estimated thermodynamic properties is used for further calculations and is provided in Table 1 along with those reported by Ogorodova et al. (2014) and Wolery and Jove-Colon (2004).

	Formula	V° (cm^3/mol)	Calculated H_f° (kJ/mol)	Fitted H_f° (kJ/mol)	S° (J/mol-K)	K0	K1	K2	K3
Sepiolite-12H_2O[1]	$Mg_8 Si_{12} O_{30} (OH)_4.12H_2O$	575.0	-20280.0	-20304.0	1349.2	696	-4726	-10394840	1377654000
Sepiolite-6H_2O[1]	$Mg_8 Si_{12} O_{30} (OH)_4.6H_2O$	569.4	-18525.9	-18468.0	1109.6	564	-3589	-10394840	1369717500
Sepiolite-4H_2O[1]	$Mg_8 Si_{12} O_{30} (OH)_4.4H_2O$	567.6	-17941.1	-17879.6	1030.0	520	-3210	-10394840	1367072000
Sepiolite-2H_2O[1]	$Mg_8 Si_{12} O_{30} (OH)_4. 2H_2O$	422.8	-17356.0	-17356.0	829.2	476	-2830	-10394840	1364426500
Sepiolite-0H_2O [1]	$Mg_8 Si_{12} O_{30} (OH)_4$	415.3	-16771.6	-16771.6	765.6	432	-2451	-10394840	1361781000
	Formula	V° (cm^3/mol)	H_f° (kJ/mol)		S° (J/mol-K)				
Sepiolite-12H_2O[2]	$Mg_8 Si_{12} O_{30} (OH)_4.12H_2O$	570	-20232.0		1226.7	-	-	-	-
Sepiolite-8H_2O[3]	$Mg_8 Si_{12} O_{30} (OH)_4.(H_2O)_4. 4H_2O$	-	-18773 ±28		1095	-	-	-	-
Sepiolite-0H_2O[3]	$Mg_8 Si_{12} O_{30} (OH)_4$	-	-16426 ±21		737	-	-	-	-

1: this study, 2: Wolery and Jove-Colon (2004), 3: Ogorodova et al. (2014)

Table 1. Standard-state thermodynamic properties. V° (molar volume), H_f° (standard molar enthalpy of formation), S° (standard molar entropy), K_0 to K_3 (heat capacity function coefficients).

The comparison of our results for the fully hydrated sepiolite end-member are in good agreement with values presented by Wolery and Jove-Colon (2004) for the V° and H°,

whereas the value of S° is slightly higher in our results. This discrepancy is attributed to the use of different values for the entropic contribution chosen in the two studies for the different oxides used to calculate the global S° of sepiolite.

The results for the $H_f°$ of Sepiolite-8H_2O by Ogorodova et al. (2014) are intermediate between our $H_f°$ values for the sepiolite-12H_2O and the sepiolite-6H_2O end-members, which is expected for an intermediatly-hydrated member. Meanwhile, calculated values for the dehydrated member are in good agreement with those presented in Ogorodova et al. (2014). The values for intermediate members cannot be compared with previous results due to the lack of available data.

3. EXPERIMENTAL METHODS

3.1 Thermogravimetric analysis

Validation of the thermodynamic model calibrated using experimental data requires a test of its capacity to reproduce the mineral assemblages observed in natural samples. The seismically active Galera Fault, SE Spain (Sánchez-Roa et al., 2016) presents a convenient example for this test.

Decomposition of sepiolite-rich fault gouge from the Galera Fault Zone was analysed in a flowing (100 cm^3/min.) air atmosphere using 851e Mettler Toledo equipment. The temperature was raised from 25 up to 1000°C at a heating rate of 20°C/min. For the measurement, a powder sample of ~23 mg was placed into an aluminium crucible, and weight loss data was collected at regular time intervals.

3.2 Strength test

The friction test of the reaction products was carried out on a triaxial deformation apparatus with a servo-controlled axial loading system and fluid pressure system (Faulkner and Armitage, 2013; Mitchell and Faulkner, 2008). The servo-controlled fluid systems

control the confining and pore fluid pressure to a resolution of 0.01 MPa, while the axial loading system has a resolution better than +/- 0.05 kN. Frictional sliding experiments were conducted on the mixture using a direct shear sample assembly (Sánchez-Roa et al., 2016). The test was performed on a crushed and sieved synthetic gouge comprised of 93 wt% talc and 7 wt% quartz, following the methods described in Sánchez-Roa et al. (2016), in order to compare strength results with those reported for the sepiolite gouge. The mixture was made into a paste using deionized water to construct a 2 mm-thick layer. Experimental conditions include: confining pressure (P_c) = 100 MPa; pore pressure (P_p) = 5 MPa; effective normal pressure (σ_{neff}) = 95 MPa; initial sliding velocity for the 1.5 mm run-in 0.3 μm/s; after the run-in, sliding velocity steps were imposed every 0.5 mm (0.3-3.0-0.3 μm/s) until a total displacement of 4 mm. The friction coefficient values (μ) were determined for each experiment as the ratio of shear stress (τ) to effective normal stress (σ_n); ($\mu=\tau/\sigma_n$).

4. RESULTS

4.1 Phase equilibrium, mineral evolution, water release and volume changes of sepiolite

This thermodynamic model based on experimental dehydration data predicts phase amounts, volume changes and water release during mineral transformations for an initial given bulk composition ($Mg_{(2)}Si_{(3)}O_{(11.5)}H_{(7)}$), corresponding to the ideal formula of sepiolite (Fig. 3). For this ideal case, a progressive decrease of Sepiolite-12H_2O from the onset of dehydration is predicted at around 100°C and is coupled with an increase in the Sepiolite-4H_2O end-member. The dehydration of zeolitic water takes place between 100 and 325°C as water progressively leaves the sepiolite structure without significant volume changes (Fig. 3). This dehydration reaction is accompanied by the release of water from the solid phase. The amount of water released during this stage is strongly conditioned by the PT-

path. In the case of a high geothermal gradient, such as PT-path I (46°C/km) in Fig. 3b, up to 4 water molecules per formula unit are lost with increasing temperature, which represent 24.6 wt% of the water in sepiolite. A lower amount of zeolitic water is lost when the geothermal gradient is lower as is the case of PT-path II (25°C/km), where only 2 water molecules are lost, representing 11.2 wt% of the water in sepiolite.

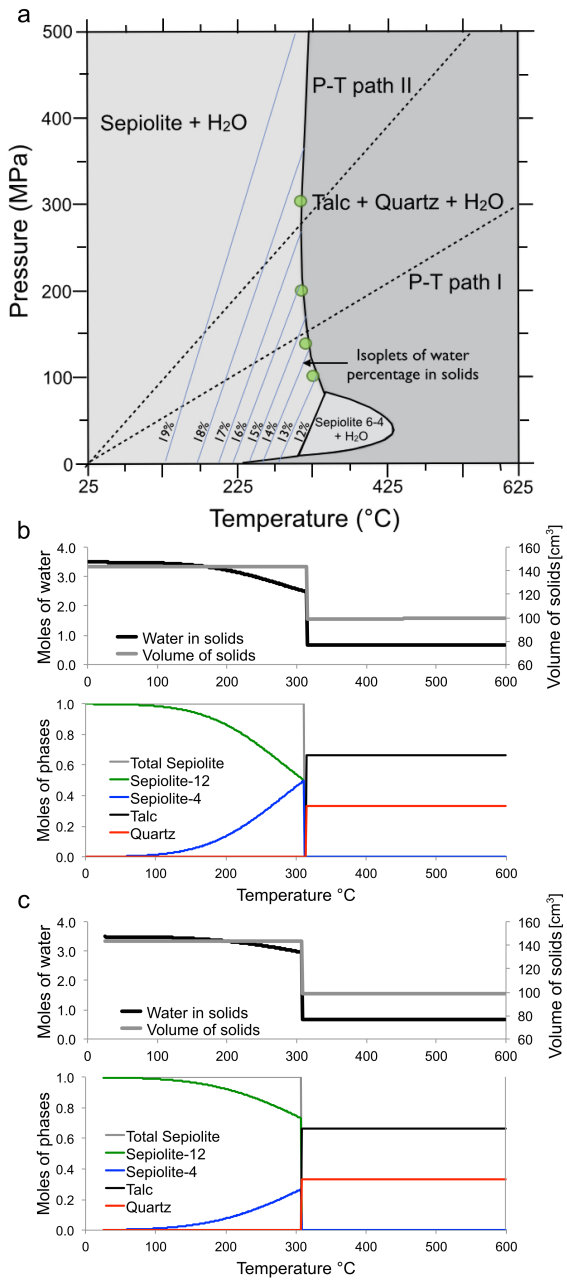

Figure 3. a. Isochemical phase diagram of an initial ideal composition of pure sepiolite in excess of water. Green dots correspond to the experimentally determined limit of reaction

sepiolite = talc + quartz + H_2O by Frank-Kamenetskiy et al. (1969). Solid blue lines correspond to isoplets of equal H_2O content indicating the percentage of water within the solid phases. Phase diagram shading is for illustrative purposes and does not reflect the variance of the mineral assemblage. b. Evolution of water content, volume of solids and mineral phases along PT-path I (46°C/km). c. Evolution of water content, volume of solids and mineral phases along PT-path II (25°C/km).

According to this model both Sepiolite-12H_2O and -4H_2O disappear at 325°C. Further dehydration states of sepiolite such as the experimentally achieved sepiolite-2H_2O and sepiolite-0H_2O (Post et al., 2007; Nagata et al., 1974) are predicted to be preceded by the metamorphic reaction 3 sepiolite = 8 talc + 4 quartz + H_2O under hydrothermal conditions, due to the thermodynamic stability of the new mineral assemblage. It should be noted that this model assumes chemical equilibrium, which may not be achieved in all natural contexts. However, the outcome of the present model is consistent with the absence of the two dehydrated phases in natural samples.

The stable mineral assemblage predicted above 325°C includes 0.66 moles of talc (93 wt%) and 0.33 moles of quartz (7 wt%) at 200 MPa, 400°C (Table 2). This reaction is accompanied by a release of 57% of the water when following PT-path I (Fig. 3b), and 71% of the water when following PT-path II (Fig. 3c). In both cases, the volume decrease of the solid phases is 31.25%.

Solid phases	N	Volume/mol	Vol (cm3)	vol%	Wt/mol	Wt (g)	Wt%	Density (g/cm3)
Talc	0.6667	137.03	91.35	92.31	379.27	252.84	92.66	2.77
Quartz	0.3333	22.82	7.61	7.69	60.08	20.03	7.34	2.63

Table 2. Stable phases predicted at 200 MPa, 400 °C and their physical properties.

The large amounts of water released during the transformation of sepiolite into talc and quartz (57% to 71% of the water in sepiolite) could have a significant impact on local pore pressures within the fault plane. In addition, the volume decrease in the fault gouge as a consequence of the transformation is substantial (31%) (Fig. 3b, 3c).

4.2 Frictional strength of the predicted mineral assemblage

Results of the friction experiment for an assemblage made of 93 wt% talc and 7 wt% quartz are compared with those obtained for a sepiolite-rich gouge (Sánchez-Roa et al., 2016) in Figure 4. The representative friction coefficient of the experiment μ=0.3 was taken at 2.49 mm of axial displacement.

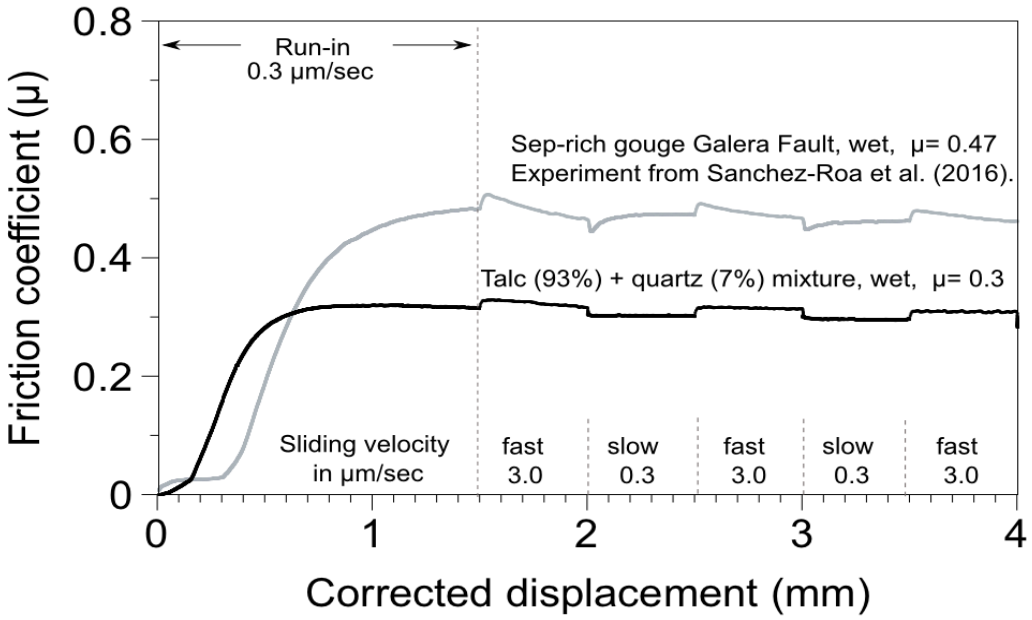

Figure 4. Experimental quantification of the frictional properties of the reaction products predicted by this model (93 wt% talc and 7 wt% quartz) under water-saturated conditions, 100 MPa confining pressure and 5 MPa pore pressure. The steps within the curves correspond to alternating changes in sliding velocity of one order of magnitude (0.3 to 3 μm/sec.). An example of a strength test on a sepiolite-rich gouge (Sánchez-Roa et al., 2016) is plotted along with our results for comparison and discussion.

Friction coefficient values for the sepiolite-rich gouge (μ=0.472) and the synthetic mixture (μ=0.3) show a contrast in strength between reactants and products (Fig. 4). Strength results for the products mixture (93 wt% talc and 7 wt% quartz) are higher than the reported value for a pure talc synthetic gouge μ=0.2 (Moore and Lockner, 2008).

4.3 Thermogravimetric analysis of the sepiolite-rich gouge from the Galera Fault Zone

Figure 5 shows a thermogravimetric analysis of the sepiolite-rich fault gouge from the Galera Fault Zone. The analysis shows five major weight losses at around 100°C, 300°C, 525°C, 728°C and 905°C which show great similarity with pure sepiolite TG analysis. In agreement with previous TG interpretations of the dehydration of sepiolite, the first loss corresponds to the dehydration of zeolitic water; the second loss corresponds to the removal of half of the water bound to the Mg atoms at the edges of the broken octahedral layer; the third loss relates to the remaining two molecules of water bound to the Mg atoms and the fourth represents the loss of the OH in the octahedral layer (Nagata et al., 1974). The poor definition of the dehydration stages after 500°C correspond to the onset of calcite and dolomite decomposition, also present in the sample, which makes the sepiolite dehydration stages slightly more difficult to identify. The last weight loss is likely to correspond to the amorphization of sepiolite and a final decomposition stage of the carbonatic minor phases.

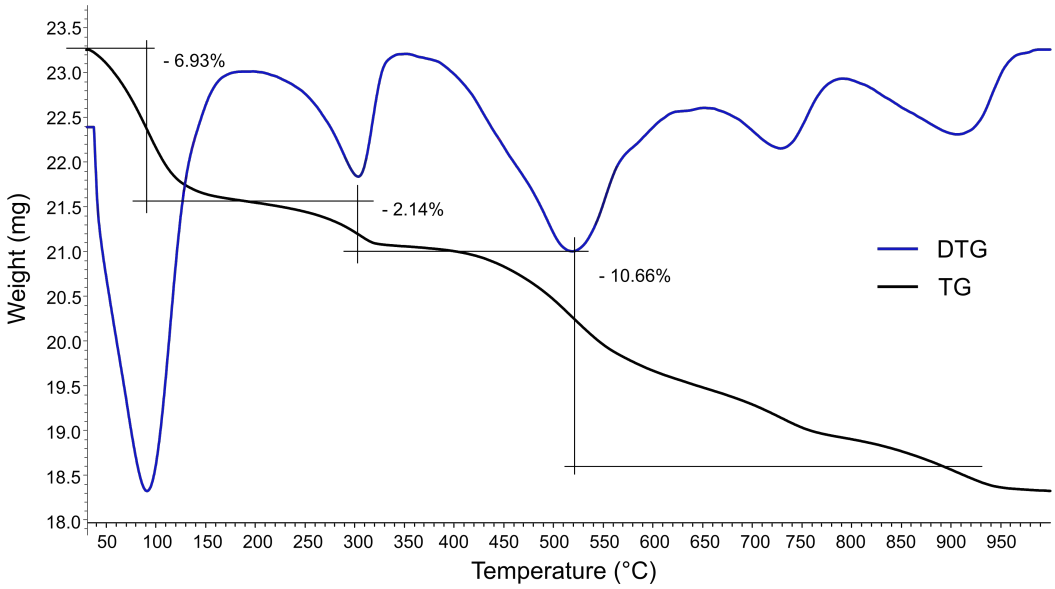

Figure 5. Thermogravimetric analysis of a natural gouge rich in sepiolite from the Galera Fault Zone (SE Spain). The four first major weight losses at around 100°C, 300°C, 525°C and 728°C coincide with those of pure sepiolite.

4.4 Model application to natural examples

The mineral assemblages of sepiolite-bearing rocks were calculated for bulk rock compositions measured by XRF analyses of sepiolite-rich rocks reported in the literature and the fault gouges from the Galera Fault Zone. The initial bulk compositions used in the calculations exclude carbonates in order to simplify the system. Nonetheless there is confidence on the model results given that water activity is not significantly affected by CO_2 at T < 375°C (Dubacq et al., 2013), and therefore the presence of carbonate in the calculation would not affect the temperature of the dehydration reaction. Figure 6 shows the isochemical phase diagrams including the newly calculated and refined thermodynamic properties for sepiolite (table 1). The calculations were performed on four examples of natural rocks, from different geological environments, containing sepiolite as an abundant stable mineral phase, including lacustrine-sepiolite (Torres-Ruiz et al., 1994) (Fig. 6a), sepiolite product of alteration of ultramafic rocks (Bonatti et al., 1983) (Fig. 6b) and two

fault gouges from the active Galera Fault Zone, the first rich in sepiolite (Fig. 6c) and the second rich in smectite (Fig. 6d).

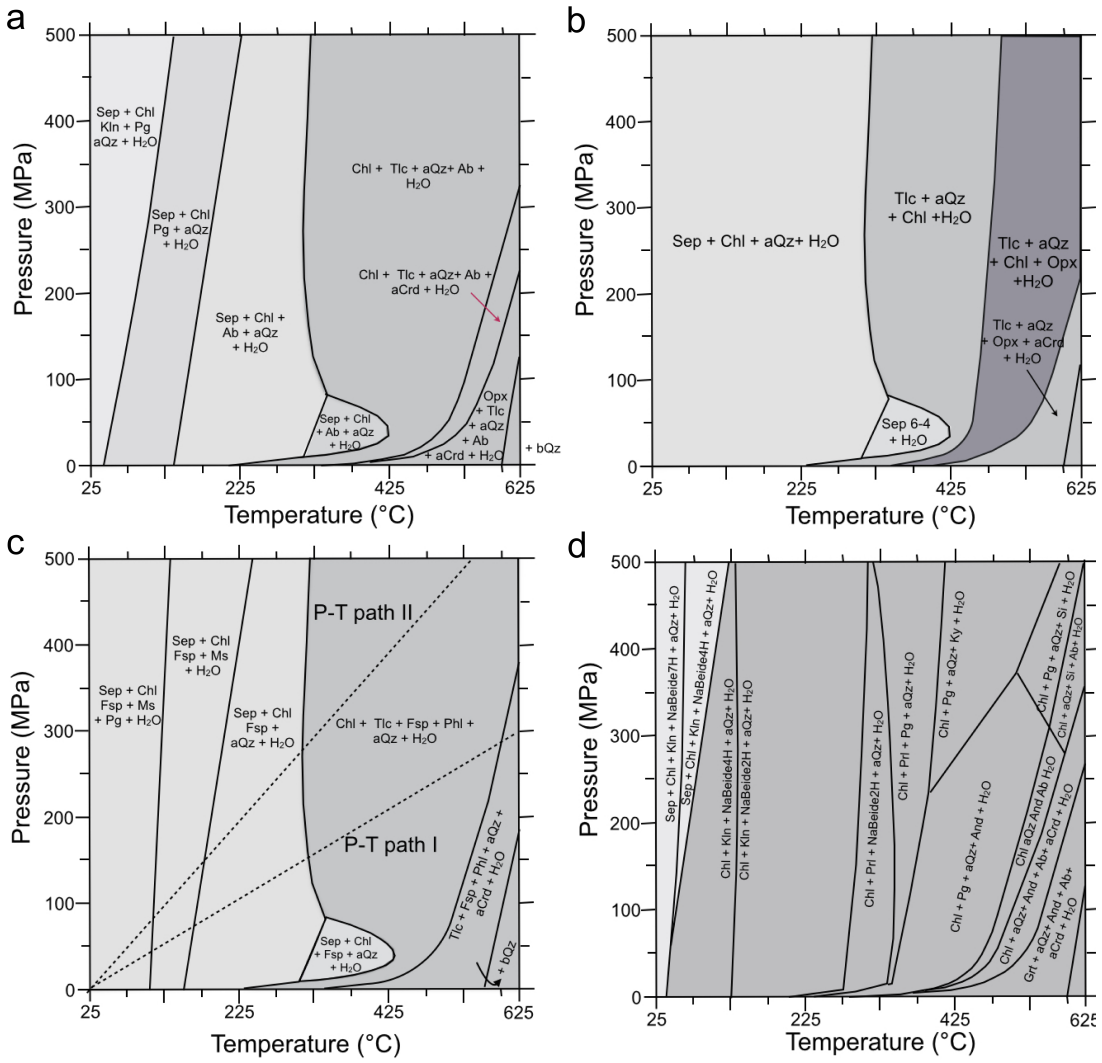

Figure 6. a. Isochemical phase diagram for a natural lacustrine-sepiolite bulk composition, from a tertiary Spanish Basin, sample Cala-4 (Torres-Ruiz et al., 1994). b. Isochemical phase diagram for natural sepiolite product of alteration of ultramafic rocks and seawater interactions within the Owen Transform Zone (Bonatti et al., 1983). c. Isochemical phase diagram for the bulk rock composition of the sepiolite-rich gouge from the deeper gouge at the central SW segment of the Galera Fault Zone. P-T paths I and II are used to calculate the water release profiles in Figure 7. d. Isochemical phase diagram for the bulk rock composition of the smectite-rich gouge from the shallower NE area of the Galera Fault

Zone. Phase diagram shading is for illustrative purposes and does not reflect the variance of the mineral assemblage. Mineral abbreviations: Ab: albite, aCrd: alpha cordierite, aQz: alpha quartz, And: andalucite, bQz: beta quartz, Chl: chlorite, Fsp: K-feldespar, Grt: garnet Ky: kyanite, Kln: kaolinite, Ms: muscovite, NaBeide2H: Na-Beidellite with a maximum of two moles of interlayer water, NaBeide4H: Na-Beidellite with a maximum of four moles of interlayer water, Opx: orthopyroxene, Phl: phlogopite, Pg: paragonite, Prl: pyrophyllite, Si: sillimanite, Sep: sepiolite, Tlc: talc and H_2O: water.

5. DISCUSSION

5.1 Validation of the model

The reaction curves representing the evolution of sepiolite with depth (Fig. 3) indicate that the metamorphic reaction 3 sepiolite = 8 talc + 4 quartz + H_2O precedes the stability of the experimentally achieved sepiolite phases such as sepiolite-2H_2O and sepiolite-0H_2O (Post et al., 2007; Nagata et al., 1974). The absence of these further dehydration states of sepiolite in nature agrees with the outcome of the calculations in this study and validates the results of this model. Furthermore, the isochemical phase diagrams calculated for the sepiolite-rich gouge predict the presence of sepiolite as the main mineral phase (>80 %; see supplementary figure 1 for the evolution of mineral phases along PT-paths I and II in Fig. 6c) followed by chlorite, feldspar, muscovite and paragonite at temperatures less than 100°C (Fig. 6c). This mineral assemblage corresponds to that identified through XRD analysis of the natural rock (Sánchez-Roa et al., 2016). Finally, the results of the model calculations for a bulk composition representative of a natural gouge mainly composed of smectite indicate a very narrow stability field of sepiolite at temperatures < 50°C, while the most abundant phase predicted by the model is Na-beidellite (Fig. 6d). These results are in agreement with the absence of sepiolite and the abundance of smectite occurring in the natural rock (Sánchez-Roa et al., 2016).

These agreements suggest that the thermodynamic properties of sepiolite derived in the present study reproduce the system behaviour within acceptable bounds. Furthermore, the model presented is consistent with the smectite model and thermodynamic data of Vidal and Dubacq (2009), and reproduce natural observations from low-grade rocks.

5.2 Case study: The Galera Fault Zone

The two clay-rich gouges analysed in this study were collected from two fault segments within the Galera Fault Zone. Their mineralogy is the product of Mg-enrichment due to hydrothermal alteration during periods of fluid-rock interaction. The hydrothermal processes in the area are concentrated within the fault planes and fractures and result in Mg-rich fault gouges. The presence of two different mineral assemblages in the area is a consequence of the evolution of a common Mg-rich fluid interacting with the wall and fault rocks. Deeper areas of the fault are affected by the Mg-rich fluid and present higher Mg-enrichment resulting in a fault gouge mainly consisting of sepiolite at the central SW segment of the fault (Rambla de los Pilares). Meanwhile, shallower sections of the fault are affected by the remaining fluid with a lower Mg-concentration. In these areas, towards the NE of the fault (Galera Village), the fault gouge consists mainly of smectite and palygorskite (Sánchez-Roa et al., 2016).

5.2.1 Sepiolite's chemical stability within fault zones

Results of the thermogravimetric analysis of the sepiolite-rich fault gouge from the Galera Fault Zone (Fig. 5) show an agreement on the temperature of the four first major weight losses with those of pure sepiolite. This correspondence demonstrates the high content and dominance of sepiolite in the fault gouge sample.

The dehydration of sepiolite is a step function that involves large and sudden volume changes related to the release of its three types of water. Figure 3 and experimental data

(Frank-Kamenetskiy et al., 1969) show that these fibrous phyllosilicates can be stable at T°< 325°C. This wide temperature-pressure range of chemical stability implies that volume changes and water release involved both in the dehydration and phase transformations of sepiolite may occur at seismogenic depths. In a geological context and specifically for fault gouge evolution, calculations of mineral transformations, volume change and water release are particularly important to determine fault strength and mechanical stability as well as potential areas where pore fluid overpressure can develop (Brantut et al., 2011).

The thermodynamic model presented in this study was used to quantify these processes in the Galera Fault area. Heat flow studies of the thermal structure of the crust in southern Spain, specifically in the Betic Cordilleras, were used to extrapolate the results to crustal processes. The study of Soto et al. (2008) predicts projected geothermal temperatures between 100 and 325°C at depths around 4 to 13 km. In this setting, the sepiolite dehydration reaction could start at depths of around 4 km, potentially increasing pore pressure values, which could in turn affect the strength of the fault plane in shallow crustal faults (Leclère et al., 2016). Sepiolite is therefore predicted to be stable and without significant structural changes, such as structure folding, up to around 13 km depth, meaning that sepiolite's physical properties such as strength (friction coefficient) may control fault gouge behaviour through most of the seismogenic depths in the Galera Fault.

Above 325°C sepiolite decomposes into the assemblage talc + quartz + H_2O and entails a major release of the water within its structure (from 57% to 71% depending on its PTº-path) (Fig. 3c), and a solid phase volume decrease of 31.25%. Both competing processes could alter the state of stress of the fault and have important implications on the stability of these clay-bearing fault planes. Furthermore, differences in the rheological properties of the gouge and the mineral assemblages after mineral reactions in depth can alter the strength of the fault plane (e.g. Leclère et al., 2016).

5.2.2 Frictional strength of sepiolite-rich gouges

Experimental friction results performed on the mineral assemblage product of sepiolite breakdown after 325ºC show a friction coefficient of 0.3 (Fig. 4). The measured friction coefficient in the modelled mixture is higher than the reported value for a pure talc synthetic gouge μ=0.2 (Moore and Lockner, 2008). The discrepancy could be related to the quartz fraction in the synthetic gouge. Quartz has significantly higher friction coefficients than talc (Moore and Lockner, 2011). This strength contrast can increase the global friction coefficient of the gouge, given that the bulk strength of polymineralic rocks depends on the proportion, shape and distribution of the minerals present (Handy, 1990, 1994; Tullis et al., 1991). Nevertheless, an approximation to the mechanical behaviour of the lithosphere is often achieved by extrapolating the properties of the weakest or the most abundant mineral phase (Huismans and Beaumont, 2003).

The velocity-dependence of talc has been shown to be velocity-strengthening and therefore mechanically stable under a wide range of temperature (25 to 400°C) and effective normal stresses (25 to 150 MPa) (Moore and Lockner, 2008). In contrast, results of the velocity dependency of strength for sepiolite-rich gouges and for pure sepiolite, show a neutral to velocity-weakening behaviour (Sánchez-Roa et al., 2016, Sánchez-Roa et al., 2017), which fulfils the prerequisite for earthquake nucleation (Marone, 1998). This strength and mechanical stability contrast between the sepiolite- and talc-rich mineral assemblages is possibly enhanced by temperature according to friction experiments on talc that have shown friction coefficients decreasing from 0.23 when sheared at room temperature, to μ<0.1 when talc is heated to 300°C and sheared at slow strain rates (Moore and Lockner, 2008). Furthermore, experiments on quartz-talc mixtures have shown that the low strength of talc is dominant in mixtures containing more than 50% talc at temperatures of 200°C (Moore and Lockner, 2011), an effect that would increase with an increasing percentage of talc as is the case of the predicted gouge in the Galera Fault containing 93 wt% talc. These

results suggest a significant decrease of the friction coefficient of the fault plane after 325°C in a Mg-rich system where sepiolite is stable at temperatures below 325ºC and the association talc + quartz + H_2O predominates above this temperature.

5.2.3 Distribution of earthquake depth in the Galera Fault Zone

The sepiolite-rich gouge is thought to be the predominant mineral assemblage of the fault rocks in the Galera Fault (Sánchez-Roa et al., 2016). According to the model presented in this study, the most significant dehydration stage for this fault gouge occurs at 325°C when sepiolite breaks down into talc + quartz + H_2O (Fig. 6c). This mineral reaction is significant and could have important implications in the rheology of the gouge and the building of overpressures on the fault plane. The link between the presence of hydrous minerals and seismogenic zones has been of particular importance for subduction zones, where studies have found a correlation between the locations of intermediate-depth earthquakes and the locations of hydrous minerals. These correlations imply that dehydration reactions are linked to the location of seismic areas (Hacker et al., 2003). To assess the effect of dehydration reactions of minerals in the Galera Fault, heat flow studies of the thermal structure of the crust in southern Spain (Soto et al., 2008) were used to calculate dehydration depths of the water release profile of the sepiolite-rich gouge and compared with the frequency of earthquake nucleation depth in the Galera Fault Zone (Fig. 7). Earthquake nucleation depth in the Galera Fault is concentrated in the shallower 13 km of the crust, while a comparatively low number of earthquakes are nucleated after 13 km depth. These nucleation depths correlate to both the thermodynamic stability of sepiolite and the water release linked to sepiolite phase transformation (Fig. 7). The distribution of earthquake depth in the Galera Fault could also partly reflect the temperature-dependent transition from frictional to viscous deformation regime for quartz, which has been indicated to occur at T° around 350°C (Kohlstedt et al., 1995; Scholz, 1998). However, the bulk composition of the fault gouges in the Galera Fault indicates

high phyllosilicate- and Mg-content making the fault gouge mineral assemblage less likely to contain significant amounts of quartz. The brittle to viscous transition in these gouges should therefore be related to the behaviour of Mg-rich mineral phases that prevail in the mineralogy of the fault gouge. According to this model, the prevailing mineral phases are predicted to be: (i). sepiolite, which is stable in the shallower 13 km (T<325ºC); and (ii) talc in areas deeper than 13 km, at temperatures higher than 325ºC and stable up to ~700ºC (Escartín et al., 2008; Moore and Lockner, 2008). Therefore, we propose that earthquake nucleation depth in the Galera Fault Zone is related to: (i) the presence of sepiolite that concentrates the majority of earthquakes in the shallower 13 km of the crust. Sepiolite is a frictionally stronger mineral phase than talc with the potential for mechanical instabilities leading to earthquake nucleation (Sánchez-Roa et al., 2017). Furthermore, sepiolite breakdown into the association talc + quartz (a weaker and mechanically stable mineral assemblage) contributes to arrest the nucleation of earthquakes at depths greater than 13 km; and (ii) the sudden water release linked to the phase transformation at around 13 km that could potentially create pore overpressures altering the state of stress on the fault plane. Both the contrasting strength of mineral assemblages and the dehydration reactions within this gouge are important factors that contribute to the distribution of the nucleation of earthquakes in the Galera Fault Zone.

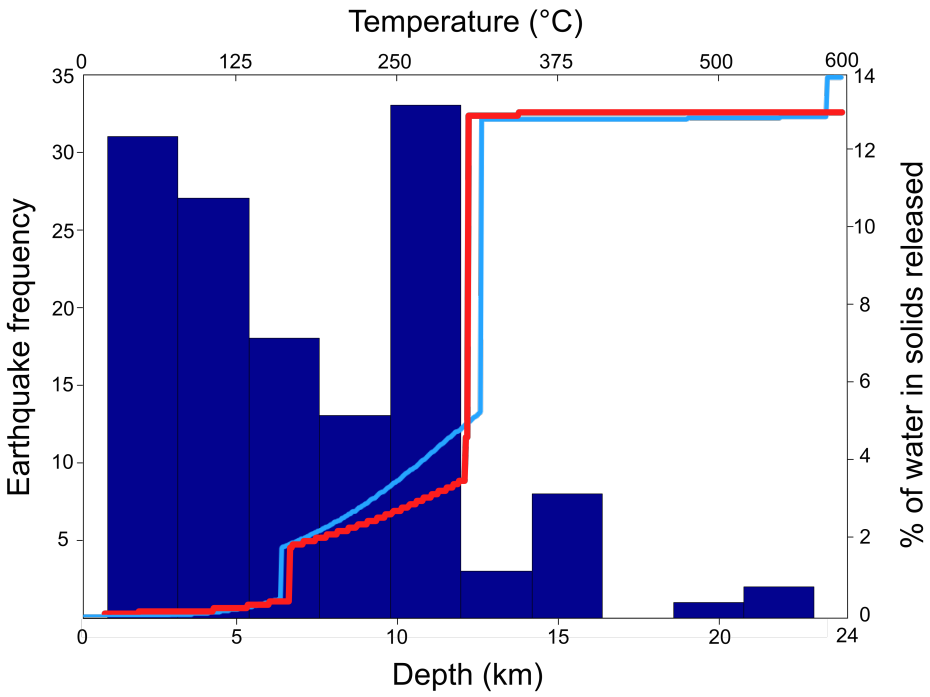

Figure 7. Frequency histogram of earthquake nucleation depth in the Galera Fault Zone, constructed with data of depth from 136 earthquakes registered by the Instituto Geografico Nacional of Spain. The spatial constraints were reduced to coordinates: latitude 37.6 to 37.9 and longitude -2.8 to -2.3. The oldest event was registered in 1863 and the most recent in July 2016. The blue line represents the water release profile for the Galera Fault gouge initial bulk composition as a percentage of H_2O in solids released by the calculated phases along P-T°-path I in figure 6c (46°C/km). The red line represents the water release profile for the Galera Fault gouge initial bulk composition as a percentage of H_2O in solids released by the initial calculated phases along P-T°-path II in figure 6c, using a geothermal gradient of 25°C per km according to Soto et al. (2008) for the Central Betics.

5. CONCLUSIONS

The thermodynamic model presented in this study allows us to approach the dehydration of sepiolite in various geological contexts including fault gouges under active deformation. According to this model and the estimated thermodynamic properties, sepiolite-$2H_2O$ and sepiolite-$0H_2O$ are not stable after 325ºC, indicating that the potential formation of the

dehydrated sepiolite species will always be preceded by the metamorphic reaction sepiolite =talc + quartz, which is the thermodynamically stable assemblage. The lack of natural occurrences of the two experimentally achieved phases validates the outcome of this model.

There could be two moments of special sensitivity when considering a fault gouge mainly composed of sepiolite; the first at the point of dehydration onset which will occur between 100 and 150°C (4 to 5 km) and will continue until the phase transformation starts. The second will take place at the onset of the mineral transformation of sepiolite into talc + quartz + H_2O between 300 and 325°C (around 13 km).

There is a reasonable agreement between the output of our model and mineral paragenesis of natural rocks containing bulk rock compositions likely to yield sepiolite content in the rock. Without sepiolite as a stable phase in the model, the starting bulk composition for the Galera Fault gouge would predict a mineral paragenesis mainly dominated by talc across the shallower 13 km of the crust that constitute the seismogenic zone in the Galera Fault Zone. Talc is one of the weakest minerals in the context of fault slip and not usually associated with seismicity. The addition of sepiolite thermodynamic properties in the calculations confirms the thermodynamic stability of sepiolite up to 325°C which, contrary to talc, has higher frictional strength and the potential for mechanical instabilities that lead to earthquake nucleation. The presence of sepiolite in Mg-rich fault gouges could contribute to unstable regimes and earthquake nucleation in an otherwise fully stable regime dominated by talc.

Acknowledgements

The authors thank the reviewers B. Dubacq and P. Lanari for their comments that led to significant improvements. This work has been supported by research projects CGL2011-30153-C02-01 and -02 from MINECO, research project UJA2014/06/17

Universidad-Caja Rural de Jaén, Research Groups RNM-179 and -325 of the Junta de Andalucía, UK NERC grant NE/J024449/1, and the F.P.I. Grant BES-2012-052 562 from the Ministerio de Economía y Competitividad of Spain. Funding assistance was provided by the Junta de Andalucía (Research Group RNM-325), University of Jaén, and project "Complex rheologic behaviour of active fault zones in carbonate multilayer sequences: applications to the estimation of seismic hazard and the exploitation of water" (University of Jaén).

REFERENCES

Bailey, S.W., 1984. Crystal chemistry of the true micas. Mineralogical Society of America Reviews in Mineralogy, 13, l3-60

Berman, R.G., 1988. Internally consistent thermodynamic data for minerals in the system Na2O-K2O-CaO-MgO-FeO-Fe2O3-Al2O3-SiO2-TiO2-H2O-CO2. J Petrol 29(2):445-522

Bonatti, E., Simmons, E.C., Breger, D., Hamlyn, P.R., Lawrence, J., 1983. Ultramafic rock/seawater interaction in the oceanic crust; Mg-silicate (sepiolite) deposit from the Indian Ocean floor, Earth Planet. Sci. Lett., 62, 229 – 238

Berman R.G., Brown T.H., 1985. The heat capacity of minerals in the system K2O–Na2O–CaO–MgO–FeO–Fe2O3–Al2O3–SiO2–TiO2–H2O–CO2: representation, estimation, and high temperature extrapolation. Contrib. Miner. Petrol. 89,168–183

Brantut, N., Sulem, J., Schubnel, A., 2011. Effect of dehydration reactions on earthquake nucleation: Stable sliding, slow transients, and unstable slip. J. Geophys. Res. 116, 1–16. doi:10.1029/2010JB007876

Brauner, K., Preisinger, A., 1956. Struktur und Entstehung des Sepioliths. Tschermaks Mineral. und Petrogr. Mitteilungen 6, 120–140. doi:10.1007/BF01128033

Chermak, J.A., Rimstidt, J.D., 1989. Estimating the thermodynamic properties (ΔG0f and ΔH0f) of silicate minerals at 298 K from the sum of polyhedral contributions. Am. Mineral. 74, 1023–1031

De Capitani, C., 1994. Gleichgewichts-Phasendiagramme: Theorie und Software. Beihefte zum Eur. J. Miner. 72. Jahr. Deutsch. Miner. Gesell 48

De Capitani, C., Petrakakis, K., 2010. The computation of equilibrium assemblage diagrams with Theriak/Domino software. Am. Mineral. 95, 1006–1016. doi:10.2138/am.2010.3354

De Capitani C., Brown T.H., 1987. The computation of chemical equilibrium in complex systems containing non-ideal solutions. Geochim Cosmochim Acta 51:2639-2652

Dubacq, B., Bickle, M.J., Evans, K.A., 2013. An activity model for phase equilibria in the H2O-CO2-NaCl system. Geochim. Cosmochim. Acta 110, 229–252. doi:10.1016/j.gca.2013.02.008

Escartín, J., Andreani, M., Hirth, G., Evans, B., 2008. Relationships between the microstructural evolution and the rheology of talc at elevated pressures and temperatures. Earth Planet. Sci. Lett. 268, 463–475. doi:10.1016/j.epsl.2008.02.004

Faulkner, D.R., Armitage, P.J., 2013. The effect of tectonic environment on permeability development around faults and in the brittle crust. Earth Planet. Sci. Lett. 375, 71–77. doi:10.1016/j.epsl.2013.05.006

Frank-Kamenetskiy, V.A., Kotov, N.V., Klochkova, G.N., 1969. Phase transformations in sepiolite and palygorskite at differrent pressures under hydrothermal conditions. Geokhimiya 14–21

García-Romero, E., Suárez, M., 2013. Sepiolite-palygorskite: Textural study and genetic considerations. Appl. Clay Sci. doi:10.1016/j.clay.2013.09.013

Gleeson, S.A., Herrington, R.J., Durango, J., Velásquez, C.A., Koll, G., 2004. The mineralogy and geochemistry of the Cerro Matoso S.A. Ni Laterite deposit, Montelíbano, Colombia. Econ. Geol. 99, 1197–1213. doi:10.2113/gsecongeo.99.6.1197

Gratier, J.-P., 2011. Fault Permeability and Strength Evolution Related to Fracturing and Healing Episodic Processes (Years to Millennia): the Role of Pressure Solution. Oil Gas Sci. Technol. – Rev. d'IFP Energies Nouv. 66, 491–506. doi:10.2516/ogst/2010014

Handy, M.R., 1990. The solid-state flow of polymineralic rocks. J. Geophys. Res., 95(B6), 8647–8661, doi:10.1029/JB095iB06p08647

Handy, M.R., 1994. Flow laws for rocks containing two non-linear viscous phases: A phenomenological approach. J. Struct. Geol., Vol 16, 3, 287–301, https://doi.org/10.1016/0191-8141(94)90035-3

Hacker, B.R., Peacock, S.M., Abers, G.A., Holloway, S.D., 2003. Subduction factory, 2, Are intermediate-depth earthquakes in subducting slabs linked to metamorphic dehydration reactions?, J. Geophys. Res., 108(B1), 2030, doi:10.1029/2001JB001129

Haines, S.H., van der Pluijm, B.A., 2012. Patterns of mineral transformations in clay gouge, with examples from low-angle normal fault rocks in the western USA. J. Struct. Geol. 43, 2–32. doi:10.1016/j.jsg.2012.05.004

Holland, T.J.B., 1989. Dependence of entropy on volume for silicate and oxide minerals: A review and a predictive model. Am. Mineral. 74, 5–13

Huismans, R.S., Beaumont, C., 2003. Symmetric and asymmetric lithospheric extension: Relative effects of frictional-plastic and viscous strain softening. J. Geophys. Res., 108, 2496, doi:10.1029/2002JB002026, B10

Kohlstedt, D.L., Evans, B., Mackwell, S.J., 1995. Strength of the lithosphere: Constraints imposed by laboratory experiments. J. Geophys. Res. 100, 17,587–17,602. doi:10.1016/S0016-0032(16)90156-X

Krekeler, M.P.S., Guggenheim, S., 2008. Defects in microstructure in palygorskite-sepiolite minerals: A transmission electron microscopy (TEM) study. Appl. Clay Sci. 39, 98–105. doi:10.1016/j.clay.2007.05.001

Leclère, H., Faulkner, D., Wheeler, J., Mariani, E., 2016. Permeability control on transient slip weakening during gypsum dehydration: Implications for earthquakes in subduction zones. Earth Planet. Sci. Lett. 442, 1–12. doi:10.1016/j.epsl.2016.02.015

Lockner, D.A., Morrow, C., Moore, D., Hickman, S., 2011. Low strength of deep San Andreas fault gouge from SAFOD core. Nature 472, 82–85. doi:10.1038/nature09927

Manning, C.E., 1995. Phase-equilibrium controls on SiO2 metasomatism by acqueous fluid in subduction zones: reaction at constant preassure and temperature. Int. Geol. Rev. doi:10.1080/00206819509465440

Marone, C., 1998. Laboratory-Derived Friction Laws and Their Application To Seismic Faulting. Annu. Rev. Earth Planet. Sci. 26, 643–696. doi:10.1146/annurev.earth.26.1.643

Mitchell, T.M., Faulkner, D.R., 2008. Experimental measurements of permeability evolution during triaxial compression of initially intact crystalline rocks and implications for fluid flow in fault zones. J. Geophys. Res. Solid Earth 113, 1–16. doi:10.1029/2008JB005588

Moore, D., Lockner, D.A., 2007. Friction of the smectite clay montmorillonite: A review and interpretation of data, in: Dixon, T.H., Moore, C. (Eds.), The Seismogenic Zone of Subduction Thrust Faults, Margins Theor. Exp. Earth Sci. Ser., Vol 2. Columbia Univ. Press, New York, pp. 317–345

Moore, D.E., Lockner, D.A., 2011. Frictional strengths of talc-serpentine and talc-quartz mixtures. J. Geophys. Res. Solid Earth 116, 1–17. doi:10.1029/2010JB007881

Moore, D.E., Lockner, D.A., 2008. Talc friction in the temperature range 25°-400°C: Relevance for Fault-Zone Weakening. Tectonophysics 449, 120–132. doi:10.1016/j.tecto.2007.11.039

Morton, N., Girty, G.H., Rockwell, T.K., 2012. Fault zone architecture of the San Jacinto fault zone in Horse Canyon, southern California: A model for focused post-seismic fluid flow and heat transfer in the shallow crust. Earth Planet. Sci. Lett. 329-330, 71–83. doi:10.1016/j.epsl.2012.02.013

Nagata, H., Shimoda, S., Sudo, T., 1974. On dehydration of bound water of sepiolite. Clays Clay Miner. 22, 285–293. doi:10.1346/CCMN.1974.0220310

Ogorodova, L., Kiseleva, I., Vigasina, M., Kabalov, Y., Grishchenk, R., Mel'chakova, L., 2014. Natural sepiolite: Enthalpies of dehydration, dehydroxylation, and formation derived from thermochemical studies. Am. Mineral., 99(11-12), pp. 2369-2373. Retrieved 10 Sep. 2017, from doi:10.2138/am-2014-4804

Post, J.E., Bish, D.L., Heaney, P.J., 2007. Synchrotron powder X-ray diffraction study of the structure and dehydration behavior of sepiolite. Am. Mineral. 92, 91–97. doi:10.2138/am.2007.2134

Ransom, B., Helgeson, H.C., 1994. A chemical and thermodynamic model of aluminous dioctahedral 2:1 layer clay minerals in diagenetic processes: regular solution representation of interlayer dehydration in smectite. Am. J. Sci. 294, 449–484.

Ratié, G., Jouvin, D., Garnier, J., Rouxel, O., Miska, S., Guimarães, E., Cruz Vieira, L., Sivry, Y., Zelano, I., Montarges‐Pelletier, E., Thil, F., Quantin, C., 2015. Nickel isotope fractionation during tropical weathering of ultramafic rocks. Chem. Geol. 402, 68–76. doi:10.1016/j.chemgeo.2015.02.039

Richard, J., Gratier, J.-P., Doan, M.-L., Boullier, A., Renard, F., 2014. Rock and mineral transformations in a fault zone leading to permanent creep: Interactions between brittle and viscous mechanisms in the San Andreas Fault. J. Geophys. Res. Solid Earth 119, 8132–8153. doi:10.1002/2014JB011489

Sánchez-Roa, C., Jiménez-Millán, J., Abad, I., Faulkner, D.R., Nieto, F., García-Tortosa, F.J., 2016. Fibrous clay mineral authigenesis induced by fluid-rock interaction in the Galera fault zone (Betic Cordillera, SE Spain) and its influence on fault gouge frictional properties. Appl. Clay Sci. doi:10.1016/j.clay.2016.06.023

Sánchez-Roa, C., Faulkner, D. R., Boulton, C., Jimenez-Millan, J., Nieto, F., 2017. How phyllosilicate mineral structure affects fault strength in Mg-rich fault systems, Geophys. Res. Lett., 44, doi:10.1002/2017GL073055

Schleicher, A.M., Hofmann, H., van der Pluijm, B.A., 2013. Constraining clay hydration state and its role in active fault systems. Geochemistry, Geophys. Geosystems 14, 1039–1052. doi:10.1002/ggge.20077

Schleicher, A.M., van der Pluijm, B.A., Warr, L.N., 2012. Chlorite-smectite clay minerals and fault behavior: New evidence from the San Andreas Fault Observatory at Depth (SAFOD) core. Lithosphere 4, 209–220. doi:10.1130/L158.1

Scholz, C.H., 1998. Earthquakes and friction laws. Nature 391, 37–42. doi:10.1038/34097

Soto, J.I., Fernandez-Ibanez, F., Fernandez, M., Antonio, G.C., 2008. Thermal structure of the crust in the Gibraltar Arc: Influence on active tectonics in the western Mediterranean. Geochemistry, Geophys. Geosystems 9. doi:10.1029/2007TC002192

Torres-Ruiz, J., López-Galindo, A., Gonzalez-Lopez, J.M., Delgado, A., 1994. Geochemistry of Spanish sepiolite-palygorskite deposits: genetic considerations based on trace elements and isotopes. Chem Geol 112:221–245

Tullis, T.E., F.G. Horowitz, Tullis, J., 1991. Flow laws of polyphase aggregates from end-member flow laws. J. Geophys. Res., 96(B5), 8081–8096, doi:10.1029/90JB02491

Vidal, O., Dubacq, B., 2009. Thermodynamic modelling of clay dehydration, stability and compositional evolution with temperature, pressure and H2O activity. Geochim. Cosmochim. Acta 73, 6544–6564. doi:10.1016/j.gca.2009.07.035

Wolery, T.J., Jove-Colon, C.F., 2004. Qualification of thermodynamic data for geochemical modeling of mineral-water interactions in dilute systems, Rep. ANL-WIS-GS-000003 REV 00, 212 pp., Bechtel SAIC, Las Vegas, Nev.

Yalçin, H., Bozkaya, Ö., 2004. Ultramafic-rock-hosted vein sepiolite occurences in the Ankara ophiolitic mélange, Central Anatolia, Turkey. Clays Clay Miner. 52, 227–239. doi:10.1346/CCMN.2004.0520209

Supplementary Figure 1: Evolution of mineral phases along a. PT-path I (46°C/km), and b. PT-path II (25°C/km) of the isochemical phase diagram for the bulk rock composition of the sepiolite-rich gouge from the deeper gouge at the central SW segment of the Galera Fault Zone.